

UCSF

UC San Francisco Electronic Theses and Dissertations

Title

Serial MRI/MRSI of Patients with Gliomas Being Treated with Novel Therapies

Permalink

<https://escholarship.org/uc/item/5rd3r5pm>

Author

Yeh, Alex

Publication Date

2014

Peer reviewed|Thesis/dissertation

Serial MRI/MRSI of Patients with Gliomas Being Treated with
Novel Therapies

by

Alex Yeh

THESIS

Submitted in partial satisfaction of the requirements for the degree of

MASTER OF SCIENCE

in

Biomedical Imaging

in the

GRADUATE DIVISION

of the

UNIVERSITY OF CALIFORNIA, SAN FRANCISCO

Copyright 2014

by

Alex Yeh

Acknowledgement

First and foremost, I would like to thank my mentor, Dr. Sarah Nelson, from whom I learned a great deal about imaging, cancer, and scientific research. I would also like to thank Qiuting Wen, Jason Crane, Beck Olson, Adam Elkhalel, and Marisa Lafontaine for helping me get familiarized with the lab. I want to thank members of the lab who were able to compile essential clinical data, namely Shauna O'Donnell and Jason Chan, who greatly simplified my work by drawing many regions of interest. I would also like to thank Dr. Peder Larson, Dr. Duan Xu, and Dr. Sabrina Ronen for taking time out of their hectic schedules to be a part of my thesis committee and provide feedback. Finally, thank you to Robert Smith, Dr. Alastair Martin, and the UCSF MSBI program for providing me with this wonderful experience.

Dedication

I would like to dedicate this to my mother, my father, and my older sister for always being so supportive and encouraging.

Serial MRI/MRSI of Patients with Gliomas Being Treated with Novel Therapies

Alex Yeh

Abstract

Background: Glioblastoma multiforme (GBM) is a primary brain tumor that typically results in poor outcomes. A number of combination therapies are being considered for improving the prognosis for such patients. In this study serial MRI data were evaluated from patients with newly diagnosed GBM who were participating in a single-arm, Phase II clinical trial for an autologous heat-shock protein peptide complex-96 (HSPPC-96) vaccine.

Methods: Patients underwent surgical resection, radiation with temozolomide, and concurrent administrations of heat-shock protein peptide complex-96 (HSPPC-96) vaccine and temozolomide. Anatomical, diffusion-weighted, and perfusion-weighted imaging parameters were examined starting after radiation therapy/temozolomide and before the first vaccine administration. Patients were imaged at regular time points thereafter. Imaging parameters were assessed for changes from baseline and for their association with overall survival (OS) and progression-free survival (PFS) using a Cox proportional hazards model.

Results: Starting at 200 days after the completion of radiotherapy, significant increases from baseline were consistently seen in both 10th percentile of the normalized apparent diffusion coefficient (nADC) and the median nADC values in the T2 hyperintense lesion. At 250-350 days from baseline, significant associations were seen for nADC values with both PFS and OS.

Conclusion: Multiparametric MR imaging provides a non-invasive method to elucidate more information about how the tumor is responding to combination therapies that include adding a novel immunotherapy vaccine to standard of care radiation and temozolomide.

Table of Contents

Introduction.....	1
Background.....	1
Diffusion-weighted Imaging (DWI).....	3
Perfusion-weighted Imaging (PWI).....	4
Materials and Methods.....	5
Patient Population.....	5
Clinical Procedure.....	6
MR Examination.....	8
Image Analysis.....	9
Statistics.....	11
Results.....	12
Patient Characteristics and Outcomes.....	12
Imaging Characteristics.....	17
Changes in Imaging Parameters.....	17
Association between Imaging Parameters and Survival.....	19
Discussion.....	23
Conclusion.....	25
References.....	27

List of Figures

Figure 1: Aligned ADC Map.	3
Figure 2: Perfusion Imaging Example.	4
Figure 3: Clinical Timeline.....	7
Figure 4: Regions of interest.....	11
Figure 5: Patient Event Chart Sorted by Overall Survival.....	12
Figure 6: Patient Event Chart Sorted by Progression-free Survival	13
Figure 7: Kaplan-Meier Curve of Progression-free Survival	14
Figure 8: Kaplan-Meier Curve of Overall Survival.....	14
Figure 9: Serial Plots.....	15
Figure 10: ADC Histograms.	16

List of Tables

Table 1: Patient Characteristics	8
Table 2: Imaging Parameters Considered	9
Table 3: Time-dependent Parameters	18
Table 4: Univariate Cox Analysis.....	20
Table 5: Multivariate Cox Analysis.....	22

Introduction

Background

Glioblastoma multiforme (GBM) is the most common type of glioma in adults, which accounts for nearly 80% of primary malignant brain tumors. In the United States, approximately 18,000 people are diagnosed with GBM, and 13,000 cancer deaths in the United States each year are attributed to GBM¹. Patients with GBM experience significant morbidity and mortality, and even though there have been advances in treatment methods, have a median survival from diagnosis of approximately 15 months². Although new combination treatments have been found to prolong survival, all patients will eventually recur, and the median survival from that point is typically only 3-6 months³.

Until recently, the Macdonald criteria, which are based on changes in cross-sectional diameters of the contrast-enhancing lesion and clinical worsening, have been used to assess tumors' progression and response to therapy⁴. Tumor progression is considered to have occurred when there is an increase of 25% or greater in the size of the contrast-enhancing lesion. There are significant limitations to the use of the Macdonald criteria because contrast enhancement, especially in post-treatment brain tumors, is non-specific and cannot reliably be used as a metric of tumor response⁵. With this in mind, an international group of neuro-oncologists reviewed findings in clinical trials and came to a consensus in defining the Response Assessment for Neuro-Oncology (RANO) criteria. These take into account changes in size of both the contrast-enhancing lesion on post-gadolinium T1-weighted MR images and the nonenhancing component of the tumor on T2-weighted/fluid-attenuated inversion recovery (FLAIR) MR images⁶.

Although these updated parameters provide useful information, recent clinical trials have shown that patients who have received standard therapies can undergo pseudoresponse, a decrease

in the size of the contrast-enhancing lesion, or pseudoprogression, an increase in the nontumoral enhancing area that are subsequently shown to be temporary effects⁷. These changes may confound the evaluation of outcome for both single and combination therapies. For example, antiangiogenic agents such as bevacizumab may cause a rapid decrease in the volume of contrast enhancement but this effect may be due to decreased permeability to the contrast agent rather than a true reduction in tumor size⁵. The development of physiological and metabolic imaging methods that can enhance the RANO criteria by adding more accurate measurements of tumor burden and by detecting biological changes in the lesion is a pressing need.

Standard treatment for GBM involves surgical resection, followed by concurrent radiation therapy and administration of temozolomide (TMZ), which is an alkylating chemotherapy agent⁸. Immunotherapy may improve outcomes in patients with GBM by causing more specific immune responses that allow for a more sustained, less toxic effect than conventional therapy³. Heat shock proteins (HSPs) are intracellular chaperones that can stimulate an immune response by delivering tumor antigens to cells presenting antigens⁹. It is hypothesized that active immunotherapy will induce the body's immune response and cause the production of tumor specific T-cells and antigens that will act against the tumor.

An autologous tumor-derived heat-shock protein peptide complex-96 (HSPPC-96) vaccine was shown to be safe for patients with recurrent GBM in a recent clinical trial³, but further study is needed to establish efficacy as a treatment for both newly diagnosed and recent lesions. The vaccine is individually prepared using a portion of the patients' own tumor that is removed during surgical resection. This study will analyze Phase II clinical trial data from patients with newly diagnosed GBM who have undergone surgical resection that removed the majority of their initial

tumor, have had tissue used to make autologous HSP vaccine and have received standard of care treatment with radiation and temozolomide.



Figure 1. Example of an aligned ADC map.

Diffusion-weighted Imaging (DWI)

Diffusion-weighted imaging (DWI) allows for quantification of the random Brownian motion of water molecules within each voxel. It is a powerful tool for evaluation of brain tumors because it provides parameters that represent the directionality and hindrance of diffusion.

Areas within the tumor that have increased cellularity will tend to have more restricted diffusion. Regions that correspond to edema will have increased water content and will therefore have less restricted diffusion. When diffusion is completely free, the average diffusion distance is proportional to the square root of the diffusion time (t) and the diffusion coefficient (D) (Equation 1)¹⁰.

$$\text{Average diffusion distance} = \sqrt{2Dt} \quad (1)$$

When diffusion is restricted, it is typically non-Gaussian and the above equation is no longer valid. This results in an underestimation of the diffusion coefficient which is known as the apparent diffusion coefficient (ADC). The ADC describes the incoherent movement of water molecule protons in the extracellular space¹¹. ADC values can be calculated on a voxel-by-voxel basis from two or more images with differing b -values, which measure the strength and length of the diffusion gradients as well as the sensitivity to diffusion (Equation 2)¹².

$$ADC = -\frac{1}{b} \ln\left(\frac{S_b}{S_0}\right) \quad (2)$$

Above, S_b and S_0 represent the signal intensities of each voxel with and without diffusion weighting, respectively. These calculations can be used to create an ADC map that can then be co-registered to anatomical images. DWI is an important tool in neurological imaging because the ADC may provide information about changes in the physiology of the tumor; with a decrease in ADC indicating a change in tumor cellularity, and an increase in ADC showing increased edema and/or a breakdown of normal tissue architecture¹¹.

Perfusion-weighted Imaging (PWI)

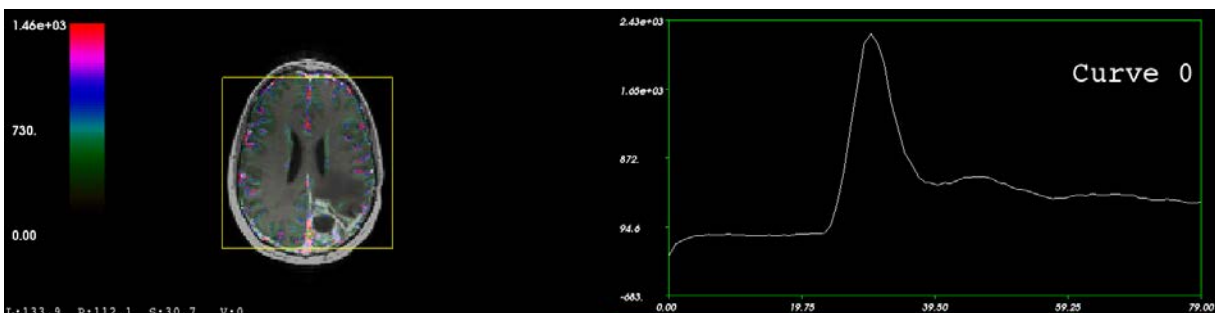


Figure 2. Example of a CBV map and peak height in a single voxel viewed using SIVIC.

The term perfusion refers to the amount of blood that is delivered to the capillary bed of tissue over a certain duration¹³. Procedures for estimating perfusion using MRI can either be exogenous, when an intravascular contrast agent is injected, or endogenous, which makes use of the signal difference between magnetically labeled and unlabeled blood. Exogenous methods include dynamic susceptibility contrast (DSC) MRI, which is the method used in this study. In this case a bolus of contrast agent, such as gadolinium, is injected into the patient's arm and a series of T2*-weighted images are taken before, during and after the injection. When the contrast agent reaches the brain it causes a reduction in signal intensity due to increased susceptibility weighting. As the agent flows through the brain vasculature the signal either returns to normal or, if there is leakage from abnormal vessels as is the case in many tumors, there will be less signal recovery. The change in the T₂* relaxation curve (ΔR_2^*) can be described using the following equation:

$$\Delta R_2^*(t) = -\frac{\ln\left(\frac{S(t)}{S_0}\right)}{TE} \quad (3)$$

In Equation 3, $S(t)$ is the T_2 or T_2^* -weighted signal at time t , S_0 is the baseline, steady-state signal, and TE is echo time. DSC is useful for imaging of brain tumors because of differences in the magnitude of the maximum signal reduction and in the amount of leakage across the blood-brain barrier. The observed ΔR_2^* can be modeled as the sum of the true R_2^* resulting from the bolus and an additional T_1 factor caused by leakage²²:

$$\Delta R_{2,observed}^*(t) = \Delta R_2^*(t) - \frac{TR \exp\left(-\frac{TR}{T_1}\right)}{TE\left(1 - \exp\left(-\frac{TR}{T_1}\right)\right)} R_1 C_{tissue}(t) \quad (4)$$

By transforming the signal using Equation 4, the problem is transformed into one of fitting the curve to estimate peak height (PH) or cerebral blood volume (CBV) and amount of signal recovery (RECOV) or a leakage factor (LF). Using non-parametric modeling, parameters were calculated directly from the $\Delta R_{2,observed}^*(t)$ curve without model-fitting¹⁵. A number of different methods have been proposed to fit DSC data and gain more insight into the physiology of the tumor. Parameters representing increased peak height and cerebral blood volume (CBV) are thought to correspond to increased blood vessel volume and more abnormal angiogenesis, whereas a lack of signal recovery or increase in leakage factor may indicate breakdown of the blood-brain barrier and higher vascular permeability^{14, 15}.

Materials and Methods

Patient Population

This Phase II, multi-center, single-arm trial enrolled participants from UCSF Department of Neurosurgery, University of Miami, Northwestern University, Johns Hopkins Hospital, The Valley Hospital, Northern Westchester Hospital, Columbia University, University of Oklahoma, and University of Pennsylvania. This study only looked at imaging data obtained from patients

who were enrolled at University of California, San Francisco (UCSF). Patients were eligible for the pre-surgery tissue acquisition portion of the study if they were over the age of 18, had a life expectancy of greater than 12 weeks, a suspected diagnosis of GBM, and were eligible for post-surgical treatment with radiotherapy and temozolomide. After the surgical resection, patients were screened to ensure that they had undergone at least a 90% resection of the contrast-enhancing tumor as measured by a postoperative MRI, T1-weighted contrast scan, or CT scan performed within 72 hours of the surgery. Patients then received standard of care radiotherapy and temozolomide and had a postoperative Karnofsky performance status of at least 70%. Participants in the study also had to have adequate bone marrow function, renal function, and liver function.

Patients were excluded from the study if they had known systemic autoimmune diseases, any prior diagnosis of any other cancer or other concurrent malignancy within the last five years with the exception of adequately treated carcinoma of the uterus or cervix or nonmetastatic nonmelanoma skin cancer, or any other planned or current use of other investigational therapies for the treatment of glioma. Patients were excluded from receiving vaccine if the post-surgery MR images indicated that progression had occurred, if they had any uncontrolled infections, if they had evidence of bleeding diathesis, or if they had unstable or severe intercurrent medical conditions. For those patients who remained in the study and received vaccine, progression was defined by the RANO criteria.

Clinical Procedure

During radiotherapy, the patients received the standard dose of 75 mg/m² of temozolomide daily during radiotherapy and completed standard external beam radiation treatment of 60 Gray that was delivered in 2 Gray fractions over a period of six weeks. Treatment with vaccine began two to five weeks after the end of radiotherapy. It was administered at 25 µg doses weekly injected

intradermally for four weeks. The fifth vaccine dose was injected two weeks after the fourth, and monthly vaccine injections began three weeks after the fifth administration and continued until the vaccine was depleted or progression occurred. Patients continued to receive standard of care temozolomide with the monthly injections. MRI and clinical evaluations were performed approximately every eight weeks to screen for progression and were continued for the full study period, 24 months from surgery, or until the disease progressed. Baseline scans were obtained for the 27 patients at an average of 16 days \pm 7 days from the end of radiotherapy.



Figure 3. Timeline of clinical procedures between surgical resection and the first vaccine administration.

Characteristics	Patients (n = 27)
Age, yr at diagnosis	
Median	55.5
Range	30-75
<40	1 (4%)
41-50	7 (26%)
51-60	10 (37%)
61-70	8 (29%)
>70	1 (4%)
Gender, n	
Male	15
Female	12
Time from diagnosis to progression, wk	(n = 19)
Median	71
Range	19 – 132
Time from stop of radiotherapy to first dose of vaccine, days	
Median	19
Range	-4 – 33
Reason for vaccine discontinuation	
Progression	14 (52%)
Completed follow-up	10 (37%)
Patient withdrew	3 (11%)

Table 1. Baseline characteristics of study subjects.

MR Examination

All MR scans were performed on a 3T GE whole body MR scanner. Anatomical imaging included a T1-weighted sagittal scout, axial T2-weighted fluid attenuated inversion recovery (FLAIR) images (repetition time (TR)/echo time (TE)/inversion time (TI) = 5850-9302/134-145/1800-2100 ms, matrix = 256 x 256 x 120, slice thickness = 1.5 mm, FOV = 24 cm x 24 cm) and pre- and post-contrast T1-weighted spoiled gradient echo (SPGR) (TR/TE = 8-9/2-8 ms, matrix = 256 x 256, slice thickness = 1.5 mm, FOV = 24 cm x 24 cm).

Diffusion-weighted images were acquired with 6-directional axial diffusion echo-planar imaging (EPI) sequences (TR/TE = 7000-12425/76-89 ms, matrix = 256 x 256 x 120, slice thickness = 1.5 mm, FOV = 24 cm x 24 cm x 18 cm, b = 1000 s/mm², NEX = 4). The ADC maps were calculated using software developed in the group, resampled to the same resolution as the

post-contrast T1-weighted images, and rigidly aligned to them with the VTK CISG software package.

Perfusion-weighted images involved collecting a series of T2*-weighted echo planar images (EPI) (TR/TE/flip angle = 1200-1500/25-45 ms/35°, matrix, slice thickness = 3-5 mm, 20 slices, 60 – 80 time points) acquired before, during, and after the injection bolus. Perfusion images were resampled to the same resolution as pre-contrast T1-weighted images and then aligned using the VTK CISG software package. Scans were obtained at baseline (post-RT and pre-vaccine) and approximately every 2 months thereafter as follow-ups.

Image Analysis

Anatomic Volumes	
T2ALL	T2 hyperintense lesion
CEL	Contrast-enhancing lesion
Diffusion Volumes	
nADC125	Volume within T2ALL lesion where nADC < 1.25
nADC15	Volume within T2ALL lesion where nADC < 1.5
Perfusion Volumes	
nCBV2	Volume within T2ALL lesion where nCBV > 2
nCBV3	Volume within T2ALL lesion where nCBV > 3
Diffusion Parameters	
nADC10	10 th percentile normalized apparent diffusion coefficient (nADC)
nADC50	Median nADC
Perfusion Parameters	
nPH50	Median normalized peak height (nPH)
nPH90	90 th percentile nPH
%Rec50	Median percentage recovery (%Rec)
%Rec10	10 th percentile %Rec

Table 2. Imaging parameters considered.

Images were transferred to a Linux workstation (Sun Microsystems, Mountain View, CA) for post-processing. Alignment between the anatomical images occurred first, and then regions of interest (ROIs) were defined corresponding to areas of hyperintensity on the FLAIR images (T2ALL) and contrast-enhancing lesion (CEL) on the post-Gadolinium T1-weighted images. The non-enhancing lesion (NEL) was calculated automatically and defined as the T2ALL lesion

subtracted from the CEL. The T2ALL and CEL ROIs were manually drawn using 3D Slicer²¹ with the aid of threshold segmentation. Volumes of these ROIs and histograms of their intensity values were generated using custom-built software. Intensity values in the T2ALL and CEL were normalized by the mode of the histogram in the (BRAIN-T2ALL = NBRAIN) ROI in order to account for differences in values between scans. From the defined lesions, volumetric, diffusion, and perfusion parameters were calculated using software developed in the Surbeck Laboratory. The parameter of interest from diffusion-weighted images was the apparent diffusion coefficient (ADC). Histograms of the ADC values within the T2ALL lesions were generated, and the histograms were found to follow an approximately normal distribution. Since many of the patients did not have CELs and also due to the small volume of many of the CELs, ADC values were not analyzed for the CELs. Cerebral blood volume (CBV), percent $\Delta R2^*$ signal recovery (Rec), $\Delta R2^*$ peak heights (PHs), and recirculation factors (RFs) were calculated for each voxel using software developed in the Surbeck Laboratory. Peak heights as well as percent recovery values were estimated with a nonparametric method¹⁵. Values were normalized to the median value within the NAWM. Perfusion peak heights and CBV maps were viewed in SIVIC²³ (Spectroscopic Imaging, Visualization, and Computing).

Statistics

Statistical analysis was performed using MATLAB R2012a (MathWorks Inc., Natick, MA). Overall survival (OS) and progression-free survival (PFS) were estimated using Kaplan-Meier survival curves from the date that the patients stopped radiotherapy. OS was determined from the date of death or last contact as of July 25, 2014. Patients who were still alive or whose statuses were unknown were censored. PFS was defined as the time span from the stop of radiotherapy to the date at which individuals progressed. Patients whose progression dates were unknown or who were either alive or lost in follow-up had censored PFS. Survival curves for different subgroups were compared using the log-rank test.

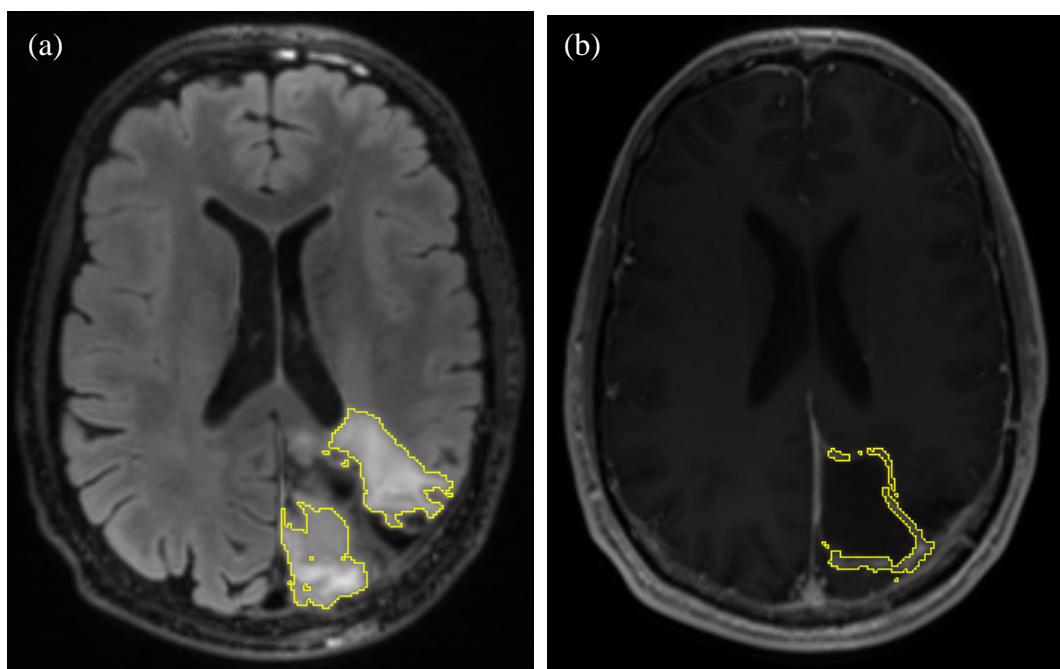


Figure 4. Regions of interest. (a) T2-weighted FLAIR image with hyperintense region (T2ALL) outlined. (b) T1-weighted contrast-enhanced lesion (CEL) outlined.

A nonparametric Wilcoxon signed-rank test was used to assess the significance of differences in values obtained at different time points, mostly between baseline and successive time points. Changes in the patients' values were assessed only if the patient had values available at both the baseline and the time point of interest.

A univariate Cox proportional hazards model was used to evaluate the influences of individual MR parameters at different time points pre-vaccination and post-vaccination on OS and PFS. The Matlab function `coxphfit` in the Statistics Toolbox was used for all Cox proportional hazards modeling. Censored patients were taken into account via an option in the function. A multivariate Cox proportional hazards model was also used to verify associations. The multivariate model assessed the same parameters as the univariate model but also took into account the patient's sex and age. For all statistical tests, a p -value of <0.05 was considered to be significant.

Results

Patient Characteristics and Outcomes

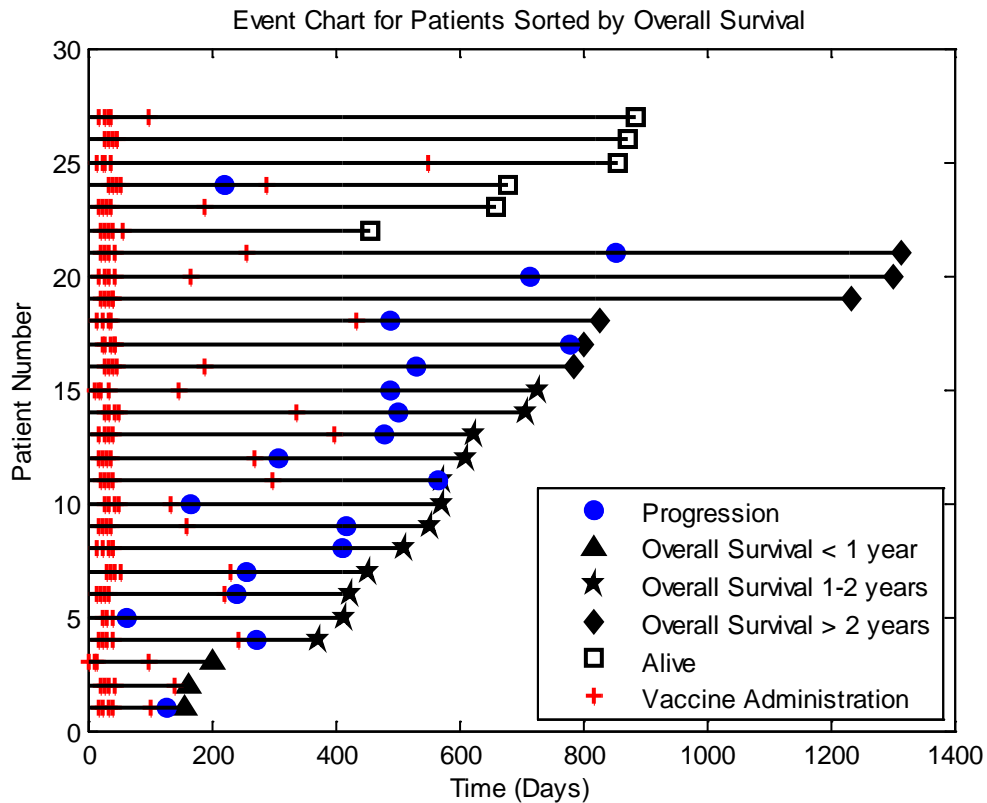


Figure 5. Patient event chart sorted by length of overall survival. Time is from the stop of radiotherapy

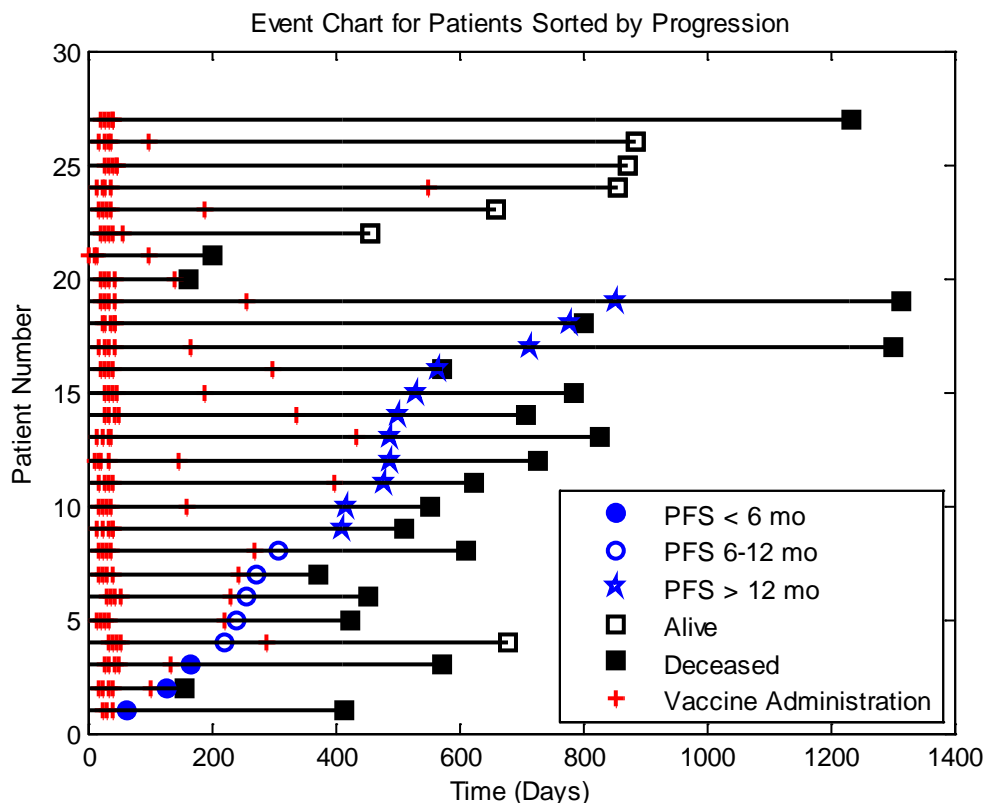


Figure 6. Patient event chart sorted by progression dates. Time is from the stop of radiotherapy.

The median OS was 683 days (95% CI, 559 – 807 days) with 6 patients censored, and the median PFS was 486 days (95% CI, 388 – 584 days) with 8 patients censored. Age or sex was not found to have a significant correlation with either OS or PFS. Using the log-rank test, there was no significant difference between the OS of patients who progressed in less than 6 months and patients who progressed between 6 and 12 months. Significant differences were found between the OS of patients who progressed in less than 6 months and patients who progressed after 6 months ($p = 0.004$, hazard ratio = 8.88) as well as patients who progressed in less than 12 months and patients who progressed after 12 months ($p < 0.001$, hazard ratio = 4.87). About 30% of the patients (8/27) progressed within a year, and about 42% of the patients (8/19) whose progression dates were known progressed within a year.

Kaplan-Meier estimate of Progression-free Survival

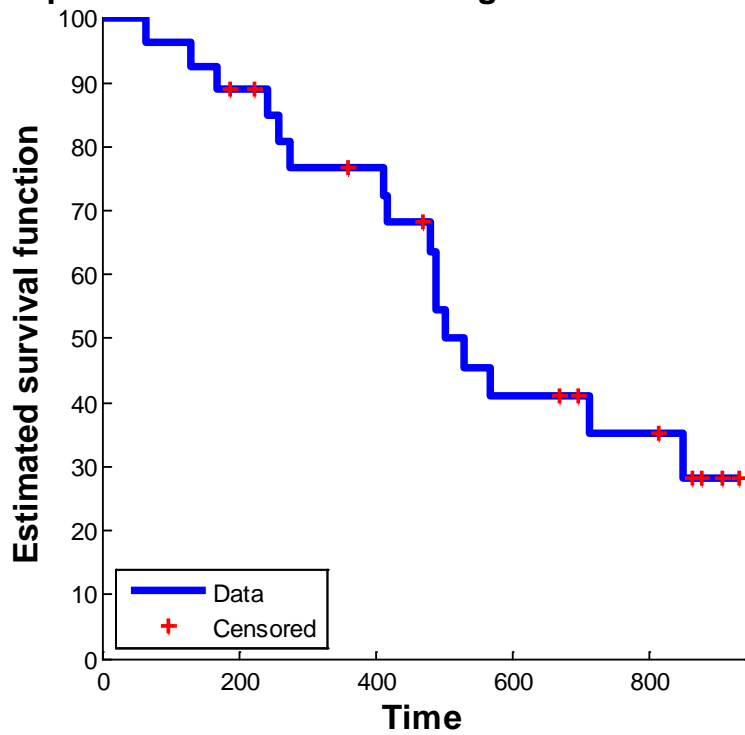


Figure 7. Kaplan-Meier survival curve of progression-free survival.

Kaplan-Meier estimate of Overall Survival

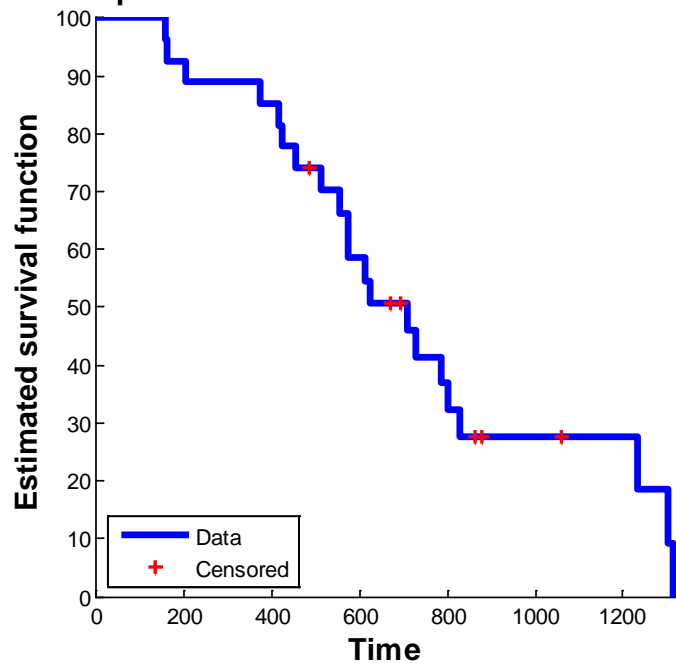


Figure 8. Kaplan-Meier survival curve of overall survival.

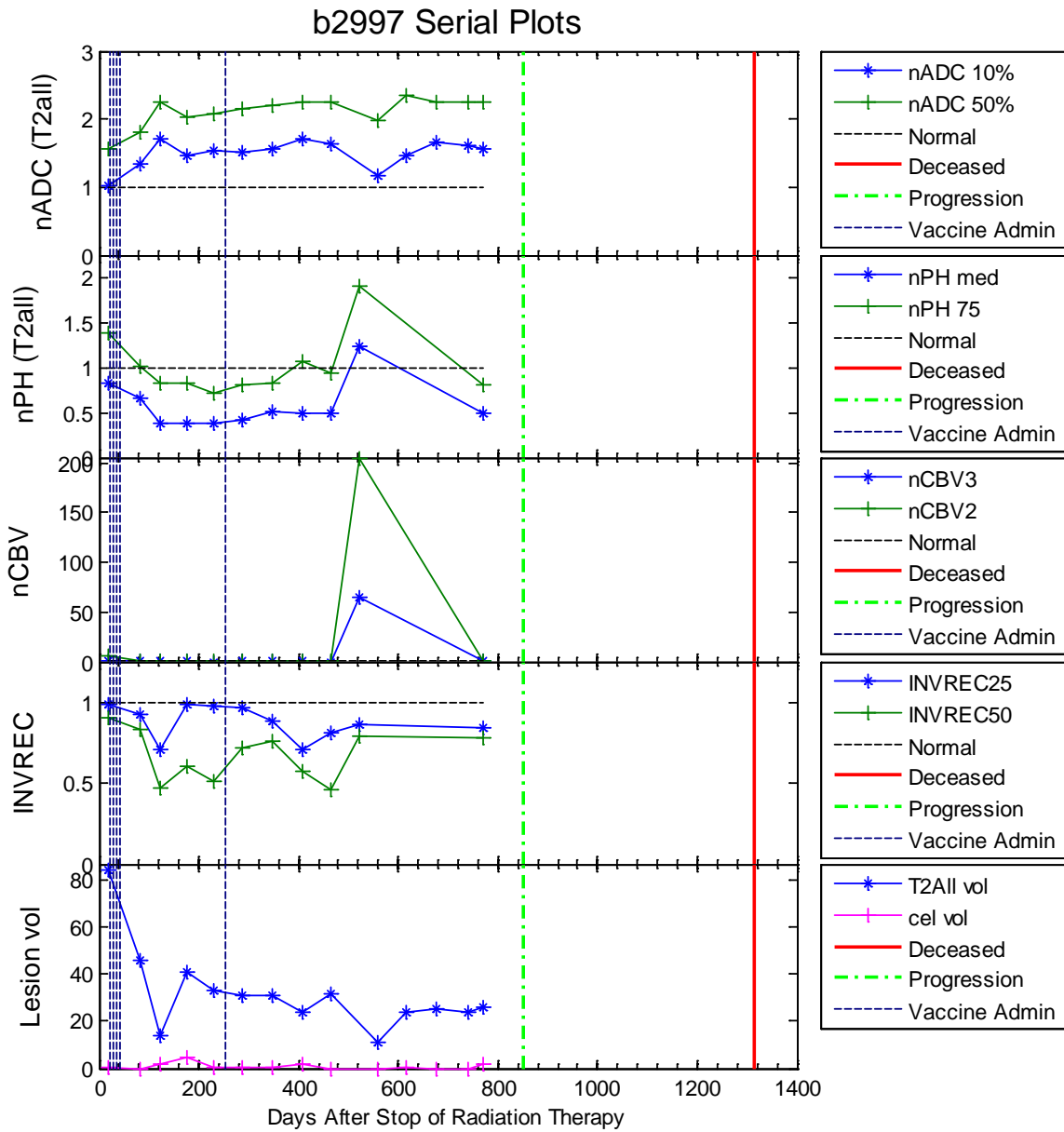


Figure 9. Serial plot with normalized ADC (*nADC*), normalized peak height (*nPH*), volumes where cerebral blood volume >2 (*nCBV2*) or >3 (*nCBV3*), recovery percentage, and lesion volumes. Vertical lines represent clinical events (vaccine administrations, progression dates, and expiration dates). This patient showed an initial decrease in volume and an increase in *nADC* values.

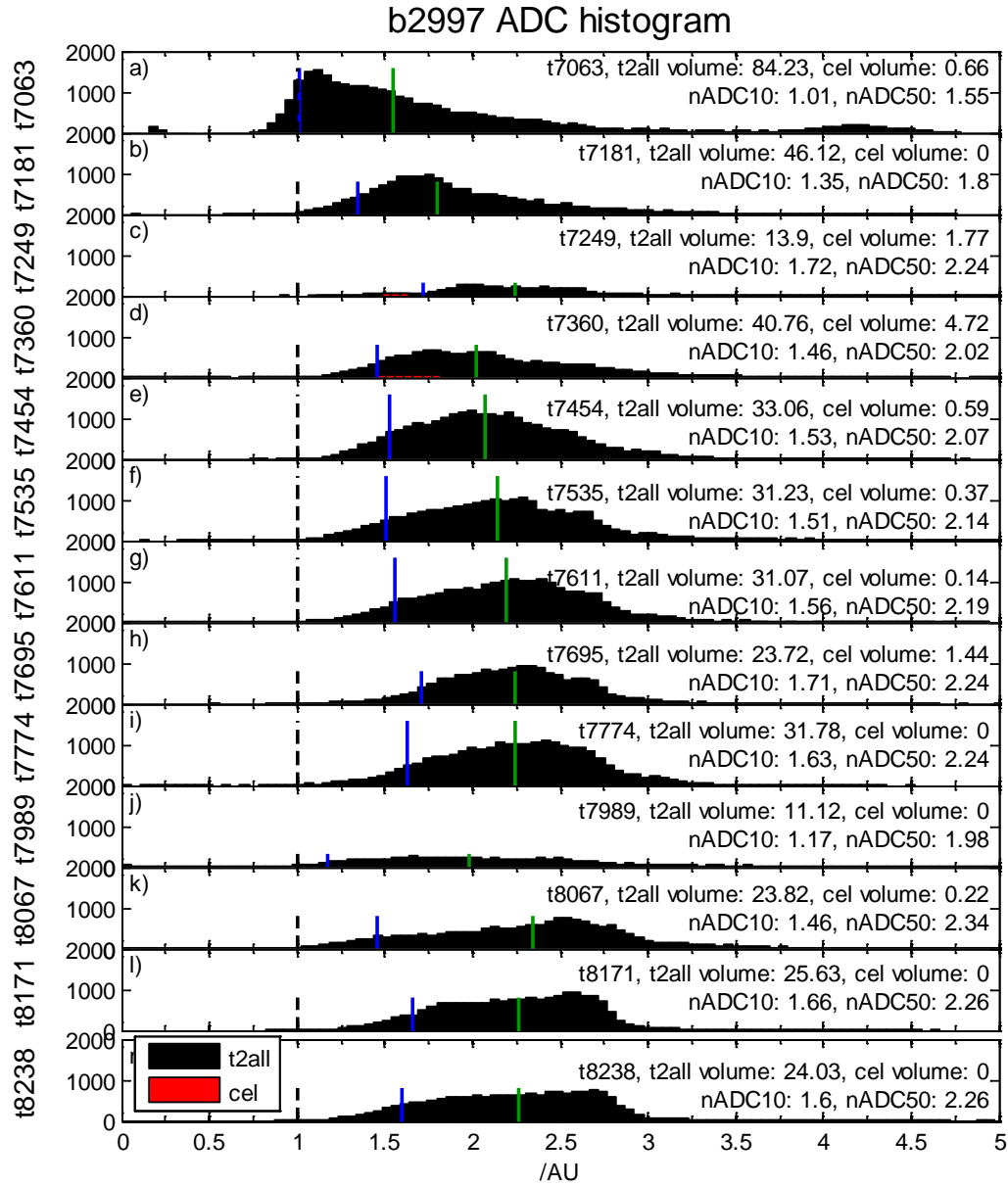


Figure 10. Histogram of normalized ADC values over time for the same patient. The blue vertical line indicates the 10th percentile nADC values, and the green vertical lines indicate median nADC values. A dotted black vertical line is present at nADC = 1. Lesion volumes and nADC values can be seen to the right of each histogram. This patient showed an initial decrease in volume and an increase in nADC values.

Imaging Characteristics

193 MR exams were acquired from 27 patients between July 2009 and August 2013. Out of these scans, 175 had DWI data available, and 161 had PWI data available. The perfusion parameters were estimated using a nonparametric fitting procedure¹⁶.

Changes in Imaging Parameters

A Wilcoxon signed-rank test was used to assess serial changes in parameters between baseline, which was considered to be after the end of radiotherapy and before the first vaccine administration, and time points thereafter. Median values, standard deviations, and the number of patients evaluated at each time point are listed in Table 2. Figure 9 shows an example of a serial plot depicting changes in several imaging parameters for a single patient. No significant changes were seen in the volumes examined except for the volume in the T2ALL lesion where normalized cerebral blood volume (nCBV) values were greater than 3 (nCBV3). Significant decreases were seen in nCBV3 volumes between baseline and follow-ups at 250-300 ($p = 0.039$) and 300-350 days ($p = 0.012$). nADC values showed an approximately normal distribution in the T2ALL lesion. There was a significant increase seen between baseline 10th percentile nADC values and values obtained between 100 and 150 days after the stop of radiotherapy ($p = 0.0125$). Significant increases in 10th percentile nADC values were seen at 200-250 days ($p = 0.02$), 250-300 days ($p < 0.001$), 300-350 days ($p < 0.01$), 350-400 days ($p = 0.04$), 400-450 days ($p = 0.02$), and 450-500 days ($p < 0.01$) after the after the stop of radiotherapy. There were also significant increases in median nADC from baseline to scans done at 200-250 days ($p = 0.04$), 250-300 days ($p < 0.01$), 300-350 days ($p < 0.001$), 350-400 days ($p = 0.04$), and 400-450 days ($p = 0.047$) from the stop of radiotherapy.

Days after RT	0-30	60-100	100-150	150-200	200-250	250-300	300-350	350-400	400-450	450-500
Anatomic Volumes (cc)										
T2ALL	<i>15.43 ± 38.82</i> n = 25	<i>16.77 ± 34.90</i> n = 17	<i>17.56 ± 52.33</i> n = 21	<i>29.18 ± 45.08</i> n = 15	<i>24.06 ± 42.97</i> n = 11	<i>17.79 ± 46.09</i> n = 13	<i>20.72 ± 46.35</i> n = 15	<i>19.93 ± 68.24</i> n = 10	<i>24.23 ± 74.21</i> n = 8	<i>22.62 ± 44.49</i> n = 9
CEL	<i>2.88 ± 6.92</i> n = 16	<i>3.05 ± 5.90</i> n = 15	<i>1.49 ± 6.95</i> n = 18	<i>2.72 ± 6.40</i> n = 12	<i>1.68 ± 4.10</i> n = 9	<i>0.69 ± 2.55</i> n = 11	<i>1.26 ± 3.71</i> n = 13	<i>1.55 ± 9.47</i> n = 10	<i>0.76 ± 8.53</i> n = 8	<i>0.078 ± 4.77</i> n = 8
Diffusion Volumes (cc)										
nADC125	<i>7.49 ± 10.08</i> n = 25	<i>3.65 ± 16.92</i> n = 17	<i>4.34 ± 5.86</i> n = 21	<i>2.8 ± 16.97</i> n = 15	<i>4.14 ± 15.79</i> n = 11	<i>1.91 ± 15.03</i> n = 13	<i>2.52 ± 14.56</i> n = 15	<i>3.98 ± 8.83</i> n = 10	<i>5.82 ± 6.76</i> n = 8	<i>3.34 ± 3.34</i> n = 10
nADC15	<i>10.07 ± 16.30</i> n = 25	<i>6.9 ± 19.36</i> n = 17	<i>10.27 ± 15.14</i> n = 21	<i>8.67 ± 22.78</i> n = 15	<i>8.07 ± 26.34</i> n = 11	<i>6.12 ± 28.26</i> n = 13	<i>5.58 ± 30.57</i> n = 15	<i>7.65 ± 30.998</i> n = 10	<i>15.71 ± 23.04</i> n = 8	<i>6.36 ± 30.03</i> n = 10
Perfusion Volumes (cc)										
nCBV2	<i>0.83 ± 3.82</i> n = 25	<i>0.70 ± 2.90</i> n = 16	<i>0.26 ± 4.01</i> n = 20	<i>0.51 ± 3.14</i> n = 15	<i>0.37 ± 1.28</i> n = 10	<i>0.19 ± 1.25</i> n = 13	<i>0.38 ± 1.42</i> n = 15	<i>0.24 ± 2.05</i> n = 10	<i>1.03 ± 1.82</i> n = 7	<i>0.15 ± 0.32</i> n = 7
nCBV3	<i>0.13 ± 1.28</i> n = 25	<i>0.14 ± 1.15</i> n = 16	<i>0.06 ± 1.08</i> n = 20	<i>0.06 ± 1.06</i> n = 15	0.02 ± 0.10 n = 10	0.01 ± 0.16 n = 13	<i>0.03 ± 0.40</i> n = 15	<i>0.02 ± 0.50</i> n = 10	<i>0.12 ± 0.26</i> n = 7	<i>0 ± 0.04</i> n = 7
Diffusion-weighted Imaging Parameters										
10 th nADC	<i>0.92 ± 0.18</i> n = 24	<i>1.01 ± 0.18</i> n = 15	1.12 ± 0.26 n = 21	<i>1.11 ± 0.21</i> n = 15	1.16 ± 0.22 n = 11	1.16 ± 0.21* n = 13	1.18 ± 0.17 n = 15	1.16 ± 0.11 n = 10	1.19 ± 0.25 n = 8	1.19 ± 0.23* n = 10
Median nADC	<i>1.39 ± 0.25</i> n = 24	<i>1.35 ± 0.26</i> n = 15	<i>1.49 ± 0.33</i> n = 21	<i>1.52 ± 0.31</i> n = 14	1.53 ± 0.27 n = 11	1.54 ± 0.29* n = 13	1.61 ± 0.24** n = 15	1.56 ± 0.18 n = 10	1.58 ± 0.30 n = 8	1.57 ± 0.28* n = 10
Perfusion-weighted Imaging Parameters										
Median nPH	<i>0.76 ± 0.25</i> n = 25	<i>0.71 ± 0.30</i> n = 16	<i>0.72 ± 0.14</i> n = 20	<i>0.69 ± 0.17</i> n = 15	<i>0.61 ± 0.10</i> n = 10	<i>0.6 ± 0.17</i> n = 13	<i>0.62 ± 0.29</i> n = 15	<i>0.61 ± 0.09</i> n = 10	<i>0.57 ± 0.13</i> n = 7	0.64 ± 0.07* n = 7
90 th nPH	<i>1.53 ± 0.85</i> n = 25	<i>1.41 ± 0.79</i> n = 16	<i>1.29 ± 0.61</i> n = 20	<i>1.39 ± 0.46</i> n = 15	<i>1.18 ± 0.33</i> n = 10	1.12 ± 0.49 n = 13	<i>1.27 ± 0.51</i> n = 15	<i>1.13 ± 0.29</i> n = 10	<i>1.39 ± 0.49</i> n = 7	1.25 ± 0.35 n = 7
Median %Rec	<i>0.85 ± 0.07</i> n = 25	<i>0.84 ± 0.06</i> n = 16	<i>0.81 ± 0.11</i> n = 20	<i>0.82 ± 0.12</i> n = 15	<i>0.82 ± 0.10</i> n = 10	<i>0.77 ± 0.08</i> n = 13	<i>0.79 ± 0.11</i> n = 15	<i>0.85 ± 0.10</i> n = 10	<i>0.80 ± 0.13</i> n = 7	<i>0.85 ± 0.17</i> n = 7
10 th %Rec	<i>0.56 ± 0.17</i> n = 25	0.65 ± 0.11* n = 16	<i>0.62 ± 0.18</i> n = 20	<i>0.66 ± 0.21</i> n = 15	<i>0.61 ± 0.20</i> n = 10	<i>0.63 ± 0.15</i> n = 13	<i>0.67 ± 0.16</i> n = 15	<i>0.64 ± 0.11</i> n = 10	<i>0.65 ± 0.19</i> n = 7	<i>0.72 ± 0.24</i> n = 7

Table 3. Median values of parameters and the number of patients whose values were available at different time points after the stop of radiotherapy. Baseline values are italicized. Time points where values show a significant ($p < 0.05$) change from baseline using the Wilcoxon signed rank test are **bolded**. * indicates $p < 0.01$, ** indicates $p < 0.001$. Parameters are defined in Table 2.

For perfusion-weighted imaging parameters, a significant decrease in median nPH (normalized peak height) values was seen at the scans performed between 450 and 500 days from baseline ($p < 0.01$). A significant decrease was seen from baseline values for the 90th percentile

nPH at 250-300 days ($p = 0.02$) and 450-500 days ($p < 0.02$). Finally, a significant increase was seen in the 10th percentile recovery percentage at the first follow-up 60-100 days after baseline ($p < 0.01$).

Association between Imaging Parameters and Survival

Using a univariate Cox proportional hazards regression, no significant association was found between baseline imaging parameters and OS or PFS. Parameters at later time points that had a significant association with either OS or PFS are shown in Table 3. At 250-300 days after the stop of radiotherapy, nADC 10th percentile ($p = 0.0306$, hazard ratio (HR) = 0.78, 95% confidence interval (CI) = 0.653-0.979) was significantly associated with PFS. nADC 10th percentile was also a strong protective factor at 300-350 days after the stop of radiotherapy for PFS ($p = 0.0081$, HR = 0.786, 95% CI = 0.658-0.940) and OS ($p = 0.0179$, HR = 0.781, 95% CI = 0.636-0.958). A higher median nADC was found to have a strong association with improved OS at 250-300 days ($p = 0.0470$, HR = 0.752, 95% CI = 0.567-0.996) and improved PFS at 300-350 days ($p = 0.0169$, HR = 0.804, 95% CI = 0.673-0.962). A higher nPH correlated with an inferior OS at 300-350 days ($p = 0.0474$, HR = 1.228, 95% CI = 1.002-1.506).

Days after stop of radiotherapy	Significant associations with overall survival	Significant associations with progression-free survival
250-300		nADC 10 th percentile in T2ALL HR = 0.800 [0.653 0.979] <i>n</i> = 13, 7 censored
	nADC median in T2ALL HR = 0.752 [0.567 0.996] <i>n</i> = 13, 7 censored	
300-350	nADC 10 th percentile in T2ALL HR = 0.781 [0.636 0.958] <i>n</i> = 13, 7 censored	nADC 10 th percentile in T2ALL* HR = 0.786 [0.658 0.940] <i>n</i> = 15, 7 censored
		nADC median in T2ALL HR = 0.804 [0.673 0.962] <i>n</i> = 15, 7 censored
	nPH median in T2ALL HR = 1.228 [1.002 1.506] <i>n</i> = 15, 7 censored	

Table 4. Univariate Cox proportional hazards regression results. Parameters at different time points that had a significant ($p < 0.05$) association with either progression-free survival or overall survival after performing univariate Cox proportional hazards regression. * indicates $p < 0.01$. HR = hazard ratio with a 95% confidence interval, and the number of patients analyzed at each time point as well as the number of censored patients are indicated.

The results of a multivariate Cox proportional hazards regression adjusting for sex and age are shown in Table 4. Although age was not a significant predictor of OS or PFS when analyzed with univariate Cox analysis, when nADC 10th percentile is included in the model, age was associated with an improved outcome for both PFS ($p = 0.0105$, HR = 0.939, 95% CI = 0.895-1.019) and OS ($p = 0.0258$, HR = 0.947, 95% CI = 0.903-1.055). nADC 10th percentile was confirmed to be a predictor for improved PFS at 250-300 days ($p = 0.0172$, HR = 0.783, 95% CI = 0.634-0.958) as well as OS at 300-350 days ($p = 0.0480$, HR = 0.652, 95% CI = 0.427-0.996) and PFS at 300-350 days ($p = 0.0043$, HR = 0.780, 95% CI = 0.658-0.925). The multivariate model also confirmed a relationship between median nADC and OS at 250-300 days ($p = 0.0435$, HR =

0.611, 95% CI = 0.379-0.986). Finally, the addition of age and sex into the model still resulted in a significant association between median nADC and PFS at 300-350 days ($p = 0.0079$, HR = 0.766, 95% CI = 0.628-0.933).

For perfusion parameters, the multivariate model yielded a significant association between median recovery (%Rec) and PFS at baseline ($p = 0.0422$, HR = 0.933, 95% CI = 0.872-0.998). Although the univariate model did not show median %Rec to be a significant predictor for improved PFS at baseline, the results trended toward significance ($p = 0.0680$, HR = 0.944, 95% CI = 0.888-1.004). The multivariate model also showed the volume in the T2ALL lesion where nADC < 1.25 to be a significant predictor of worse OS ($p = 0.0480$, HR = 1.163, 95% CI = 1.001-1.352). Although the univariate model did not show a significant association between this parameter and OS, there was a definite trend ($p = 0.0970$, HR = 1.106, 95% CI = 0.982-1.246).

Days after stop of radiotherapy	Significant associations with overall survival	Significant associations with progression-free survival
Baseline (0-30)	Age (nADC 10 th % and sex) HR = 0.947 [0.903 1.055] <i>n</i> = 24, 8 censored	Age (nADC 10 th % and sex) HR = 0.939 [0.895 1.019] <i>n</i> = 24, 8 censored
		%Rec median (age and sex) HR = 0.933 [0.872 0.998] <i>n</i> = 25, 8 censored
150-200	Volume in T2ALL where nADC < 1.25 (age and sex) HR = 1.163 [1.001 1.352] <i>n</i> = 15, 8 censored	
250-300		nADC 10 th % (age and sex) HR = 0.783 [0.640 0.958] <i>n</i> = 13, 7 censored
	nADC median (age and sex) HR = 0.611 [0.379 0.986] <i>n</i> = 13, 7 censored	
300-350	nADC 10 th % (age and sex) HR = 0.652 [0.427 0.996] <i>n</i> = 15, 7 censored	nADC 10 th % (age and sex)* HR = 0.780 [0.658 0.925] <i>n</i> = 15, 7 censored
		nADC median (age and sex)* HR = 0.766 [0.628 0.933] <i>n</i> = 15, 7 censored

Table 5. Multivariate Cox proportional hazards regression results. The statistically significant parameter is listed, with the other parameters included in the model listed in parantheses. Parameters at different time points that had a significant ($p < 0.05$) association with either progression-free survival or overall survival after performing multivariate Cox proportional hazards regression. HR = hazard ratio, and the number of patients analyzed at each time point as well as the number of censored patients are indicated.

Discussion

Treatment of GBM still leaves much to be desired. Recently developed treatments have been unable to provide significant extensions of life, and current options such as radiation therapy and chemotherapy may cause a decrease in quality of life for patients due to side effects such as cognitive impairment. Since immunotherapy recruits the body's immune system to target tumor cells, it may be able to provide a specific yet nontoxic alternative. MRI is a powerful tool that is essential for providing information that can be used to evaluate response to therapy. This study aims to examine serial anatomic, diffusion-weighted, and perfusion-weighted imaging parameters in patients who have received an autologous HSPPC-96 vaccine. The goals of the study include determining whether these parameters can be used to assess changes in tumor characteristics corresponding to response to immunotherapy as well as whether parameters that are able to predict PFS and OS.

The volume of pixels within the T2 hyperintense lesion that have cerebral blood volume (nCBV) values of greater than 3 times that in normal appearing brain saw a significant decrease at follow-ups performed between 250-300 and 300-350 days after the stop of radiotherapy. This indicates that there were fewer areas in the T2 hyperintense lesion with elevated CBV. Prior studies have indicated that nCBV correlates with the higher vascularity that is typically observed in high grade gliomas¹⁷. The reduction in the volume with high nCBVs agrees with the finding that there is a decrease in normalized peak heights. These results suggest that the concurrent immunotherapy and chemotherapy cause a reduction in vascular density and it seems reasonable to interpret this as a positive effect of the treatment. Univariate Cox analysis also shows that a higher median nPH at 250-300 days after the stop of radiotherapy is associated with poorer OS. A previous study also showed an association between higher nPH and shorter PFS¹⁶. Multivariate

Cox analysis indicated that there is a significant association between higher median recovery percentage at baseline and longer PFS. As previous work has shown that the recovery percentage is lower in the contrast-enhancing lesion¹⁵, it is logical that a high recovery percentage would be associated with a longer PFS.

Normalized ADC values showed a significant increase from baseline starting at 200 days after radiotherapy for both 10th percentile and median values. The 10th percentile values indicated that there was an additional significant increase from baseline scans to those performed at 100-150 days after radiotherapy. It is expected that the 10th percentile may be more sensitive than the median in assessing regions of the tumor that are changing as it reflects the most abnormal region. Reduced nADC values are typically assumed to reflect increased cellularity, whereas increased nADC may reflect the formation of edema or other treatment effects¹⁸. The observed increase in nADC values agree with previous studies showing radiation therapy to be associated with a disruption of tissue architecture a decrease in cellularity; these effects may be due to treatment-induced necrosis¹⁹. Time-dependent analysis yielded an association with both OS and PFS at the time periods between 250 and 350 days after baseline. Our nADC histograms in the T2ALL lesion showed that the distribution of nADC values were approximately normal.

The surgical resection may cause ischemia around the resection cavity, and there may be temporarily reduced ADC values that return to normal after around 90 days²⁰. The median days from surgical resection to the baseline scan in the patient cohort was 97 days, indicating that most of the patients were imaged sufficiently long enough after surgery for the effects of ischemia to have been resolved. Even though the ADC values were lower at the baseline than in following scans, it is thus not likely that they were due to the temporary reduction of ADC values seen immediately after surgery. Another potential confounding factor for ADC values is radiotherapy-

induced edema. It can be difficult to distinguish between recurrent GBM and radiation necrosis, as either edema resulting from radiation or gliosis associated with a recurrent tumor may result in elevated ADC values. The significant increases in ADC and associations with survival in our study were seen at time points between 250 and 350 days after the stop of radiotherapy. The long period of time between the radiation therapy and these time points may reduce the confounding effects of radiation necrosis or edema.

As this is an exploratory study, the number of patients is relatively small ($n = 27$). Furthermore, the follow-up scans were not performed at rigidly defined dates, so splitting up the follow-up scan events into time ranges further reduced the sample size. Although multivariate analysis took into account sex and age, Karnofsky performance statuses were unavailable. Additional parameters such as extent of resection, amount of edema, midline shift, and location of the tumor were not examined. Some of the patients underwent additional treatments such as bevacizumab (Avastin) and/or lomustine (CCNU) at the time of recurrence..

Conclusion

In conclusion, our study explores the effects that a novel immunotherapy may have on survival and MRI parameters of newly diagnosed GBM patients. Significant and sustained ADC increases were seen, and an association between both median and 10th percentile ADC and survival was found. The increase in ADC values is consistent with the hypothesis that the immunotherapy has some treatment effect on the tumor. Increased ADC values indicate that a breakdown of the cellular architecture of the tumor may be occurring. This study highlights the potential usefulness of using ADC to assess patient response to novel treatments and to help in resolving confounding effects that are observed with standard anatomic imaging. Perfusion-weighted imaging parameters showed some significant and near-significant results, but further analysis would be needed to

determine whether these results hold up in a larger population of patients. Our study indicates that multiparametric MR examinations that combine anatomic, diffusion, and perfusion information are a useful tool for predicting outcomes, as well as analyze response to therapies in patients with GBM being treatment with combination therapy.

References

1. Schwartzbaum JA, Fisher JL, Aldape, KD, et al. Epidemiology and molecular pathology of glioma. *Nature Clinical Practice Neurol*. 2006;2:494-503.
2. Stupp R, Mason WP, van den Bent MJ, et al. Radiotherapy plus concomitant and adjuvant temozolomide for glioblastoma. *N Engl J Med*. 2005;352:987-996.
3. Bloch O, Crane CA, Fuks, Y et al. Heat-shock protein peptide complex-96 vaccination for recurrent glioblastoma: a phase II, single-arm trial. *Neuro-Oncol*. 2014;16:274-279.
4. Macdonald DR, Cascino TL, Schold SC, Jr, Cairncross JG. Response criteria for phase II studies of supratentorial malignant glioma. *J Clin Oncol*. 1990;8:1277-1280.
5. Hygino da Cruz Jr LC, Rodriguez I, Domingues RC, et al. Pseudoprogression and Pseudoresponse: Imaging Challenges in the Assessment of Posttreatment Glioma. *American Journal of Neuroradiology*. 2011;32:1978-1985.
6. Wen PY, Macdonald DR, Reardon DA, et al. Updated response assessment criteria for high-grade gliomas: Response Assessment in Neuro-Oncology working group. *J Clin Oncol*. 2010;28:1963-192.
7. Taal W, Brandsma D, de Bruin HG, et al. Incidence of early pseudoprogression in a cohort of malignant glioma patients treated with chemoradiation with temozolomide. *Cancer*. 2008;113:405-410.
8. Crane CA, Han SJ, Ahn B, et al. Individual Patient-Specific Immunity Against High-Grade Glioma after Vaccination with Autologous Tumor Derived Peptides Bound to the 96 KD Chaperone Protein. *Clin Cancer Res* 2013;19:205-214.
9. Srivastava PK, Callahan MK, Mauri MM. Treating human cancers with heat shock protein-peptide complexes: the road ahead. *Expert Opin Biol Ther*. 2009;9:179-186.
10. Wen Q. Diffusion Imaging. (2014, July 20). Presentation given at University of California, San Francisco.
11. Wen Q, Jalilian L, Lupo JM, et al. Comparison of ADC metrics and their association with outcome for patients with newly diagnosed glioblastoma being treated with radiation therapy, temozolomide, erlotinib and bevacizumab. Unpublished manuscript, University of California, San Francisco 2014.
12. Graessner J. Frequently Asked Questions: Diffusion-Weighted Imaging (DWI). *MAGNETOM Flash*. January 2011. Siemens Healthcare, Hamburg, Germany.
13. Lupo J. Perfusion-Weighted MRI. (2014, July 21). Presentation given at University of California, San Francisco.
14. Lee MC, Cha S, Chang SM, Nelson SJ. Dynamic susceptibility contrast perfusion imaging of radiation effects in a normal-appearing brain tissue: changes in the first-pass and recirculation phases. *J Magn Reson Imaging*. 2005; 21:683-693.
15. Lupo JM, Cha S, Chang SM, Nelson SJ. Dynamic susceptibility-weighted perfusion imaging of high-grade gliomas: characterization of spatial heterogeneity. *ANJR Am J Neuroradiol*. 2005; 26:1446-1454.
16. Li Y, Lupo JM, Polley MY, et al. Serial analysis of imaging parameters in patients with newly diagnosed glioblastoma multiforme. *Neuro-Oncology* 2011;13(5):546-557.
17. Sugahara T, Korogi Y, Kochi M, et al. Correlation of MR imaging-determined cerebral blood volume maps with histologic and angiographic determination of vascularity of gliomas. *AJR Am J Roentgenol*. 1998; 171(6):1479-1486.

18. Kono K, Inoue Y, Nakayama K, et al. The Role of Diffusion-weighted Imaging in Patients with Brain Tumors. *AJNR Am J Neuroradiol* 2001; 22:1081-1088.
19. Plowman PN. Stereotactic radiosurgery. VIII. The classification of postradiation reactions. *Br J Neurosurg*. 1999; 13:256-264.
20. Smith JS, Cha S, Mayo MC, et al. Serial diffusion-weighted magnetic resonance imaging in cases of glioma: distinguishing tumor recurrence from postresection injury. 2005 Sep; 103(3):428-438.
21. Egger J, Kapur T, Fedorov A, et al. GBM Volumetry Using the 3D Slicer Medical Image Computing Platform. *Nature Scientific Reports* 2013; 3:1634.
22. Essock-Burns E. Integration of Physiologic MRI to Improve Antiangiogenic Treatment Management for Patients with Glioblastoma. Doctoral dissertation. University of California, San Francisco and University of California, Berkeley. 2012 June.
23. Crane JC, Olson MP, Lupo JM, et al. Visualization and Analysis of Dynamic MRSI and Perfusion MRI Using the Open-Source SIVIC Software Framework. ISMRM Abstract. 2011.

